Viscous Transonic Airfoil Workshop Compendium of Results

Terry L. Holst
NASA Ames Research Center, Moffett Field, California

Introduction

DURING the past three years, the Viscous Transonic Airfoil (VTA) Workshop, sponsored by the AIAA Fluid Dynamics Technical Committee, has been planned and organized. The workshop implementation is in two parts. The first part consisted of presentations at the AIAA 25th Aerospace Sciences Meeting at Reno, NV, in Jan. 1987 by 15 author groups with a variety of different viscous airfoil numerical methods.[1-16] The second part is this compendium of results, where the individual contributions have been combined in a format to facilitate comparisons among both the various computations and selected experimental data.

The individual author groups have computed a set of results for test cases involving three different airfoils: the classical NACA 0012 airfoil, the RAE 2822 supercritical airfoil, and a recently produced airfoil called the Jones airfoil. The test cases included a variety of different situations ranging from attached subcritical flows to transonic flows with both shock-induced and angle-of-attack-induced separation. A complete set of instructions given to each author group, which lists all of the requested airfoil cases, required results, and result format, is reproduced in Ref. 17.

The methods used by the various authors vary from momentum-integral boundary-layer methods, coupled with transonic potential inviscid codes to full Navier-Stokes methods. A quick-reference table showing authors, paper references, and methods used is given in Table 1. A total of 23 different sets of results were submitted by the 15 author groups, as several authors decided to submit several sets of results. The majority of methods (a total of 16) utilize the Navier-Stokes equations. This is in direct contrast to the situation in 1980–81 at the Stanford Workshop on Complex Turbulent Flows,[18] where very limited results on airfoil calculations were submitted with Navier-Stokes methods. This suggests a strong trend toward the Navier-Stokes formulation, even though it can be computationally expensive. The remaining formulations are split between several categories: two are Euler/boundary-layer methods, and five are potential/boundary layer methods. The boundary-layer methods are divided between the momentum integral approach and the full boundary-layer equation approach.

Major objectives to be addressed in this compendium of results include 1) establishment of the abilities of viscous airfoil analysis methods to predict aerodynamic trends, and 2) establishment of the qualitative abilities of the various methods for predicting details of viscous airfoil flowfields, including drag. In short, the primary objective of the VTA Workshop is CFD computer code validation.

There are two types of errors that the validation process seeks to identify and hopefully eliminate. These include physical model errors and numerical errors. The physical models associated with CFD applications include the governing equations, the viscosity law, boundary conditions, the equation of state, and the turbulence model. Numerical errors associated with CFD applications are due to time and space discretization schemes, boundary condition implementation schemes, grid resolution, grid stretching, and artificial dissipation. Differences between two computed results that use different physical models are best evaluated by using accurate experimental data. Differences between two computed results that use the same physical models have to be numerical in nature by definition. Numerical errors can be effectively identified by numerical solution-to-solution comparisons. Grid refinement studies, outer boundary position studies, and code-to-code comparisons are examples of this type of error evaluation scenario. In actual practice, physical model and numerical errors coexist in most applications. Thus, identification, evaluation, and removal of errors associated with CFD applications are best accomplished by a combined implementation of experimental and solution-to-solution comparisons. The purpose of the VTA Workshop in general, and this compendium of results in particular, is to achieve this type of comprehensive code validation for the viscous transonic airfoil problem.

Discussion of Results

The results presented herein are divided into three sections, one section for each of the three airfoils studied. The Workshop Call for Papers asked for a total of 37 curves, including pressure distributions, drag vs Mach number, lift vs drag, skin-friction distributions, and many more. Each curve was assigned a priority to guide the authors who had limited

Terry L. Holst received his Ph.D in Aerospace and Mechanical Engineering from Iowa State University in 1975. He is currently Chief of the Applied Computational Fluids Branch at NASA Ames Research Center and has been involved with research in the field of Computational Fluid Dynamics for the past 18 years. He has developed algorithms and codes for applications in the transonic, supersonic, and hypersonic speed regimes utilizing the potential, Euler, and Navier-Stokes governing equation formulations. He is an Associate Fellow of AIAA.

Presented as Paper 87-1460 at the AIAA 19th Fluid Dynamics, Plasma Dynamics and Lasers Conference, Honolulu, HI, June 8-10, 1987; received July 8, 1987; revision received Aug. 12, 1987.

computational resources so that the cases deemed more important would receive more emphasis. As a result of this approach (and because certain cases were not computable by some of the methods), not every author group submitted results for each curve. Out of a total possible 851 curves (37 requested curves times 23 methods), a total of 491 curves were submitted. In the interest of brevity, only a subset of the total number of available curves is presented. Additional results are presented in Ref. 17.

NACA 0012 Airfoil Cases

The NACA 0012 airfoil is a symmetric, 12% thick airfoil that has an analytical definition given in Ref. 17. This airfoil, while not being state-of-the-art in airfoil design, is extremely valuable as a standard because it has been tested extensively both experimentally and computationally. As a consequence, a range of experimental results taken from various sources can be compared with the present range of computational results.

The first results for the NACA 0012 airfoil are pressure coefficient distributions at $M_\infty = 0.7$, $\alpha = 1.49$ deg, and $Re_c = 9 \times 10^6$. These results, including 20 separate curves, are presented in Fig. 1 on a single set of axes without labels. For this case, the flow is attached and just slightly supersonic near the leading-edge upper surface. All methods produce very similar results with very little scatter and are in excellent agreement with the experimental data of Harris.[19] The measured experimental angle of attack for this case was 1.80 deg. Using a linear method for simulating wind-tunnel-wall interference, Harris determined the corrected angle of attack to be 1.49 deg. This is the angle of attack used to compute all the results displayed in Fig. 1. The consistency and accuracy of results for this case indicate that, at least for surface pressure associated with attached, weakly transonic flow, computational methods have attained a sophisticated level of development.

The second set of results computed for the NACA 0012 airfoil also consists of pressure coefficient distributions and is displayed in Fig. 2. These calculations were performed for $M_\infty = 0.55$, $\alpha = 8.34$ deg, and $Re_c = 9 \times 10^6$. Again, the angle of attack used in the computations (8.34 deg) is the corrected value obtained by Harris from the measured value (9.86 deg) using a linear analysis for wind-tunnel-wall effects. For this case, the flow has a supersonic bubble well forward on the airfoil upper surface and is slightly separated at the foot of the shock. In addition, several authors reported boundary-layer separation at the airfoil trailing edge. The angle of attack for this case is about 1 deg below the maximum lift value.

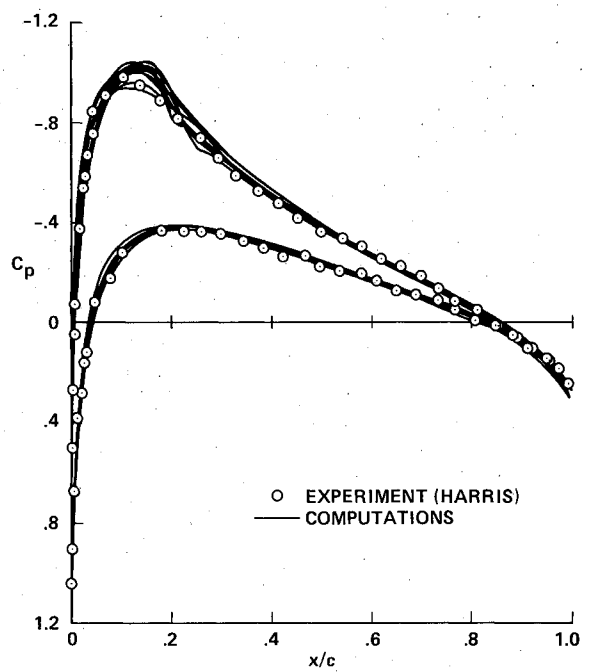

Fig. 1 Comparison of pressure coefficient distributions for the NACA 0012 airfoil, $M_\infty = 0.70$, $\alpha = 149$ deg (corrected), $Re_c = 9.0 \times 10^6$.

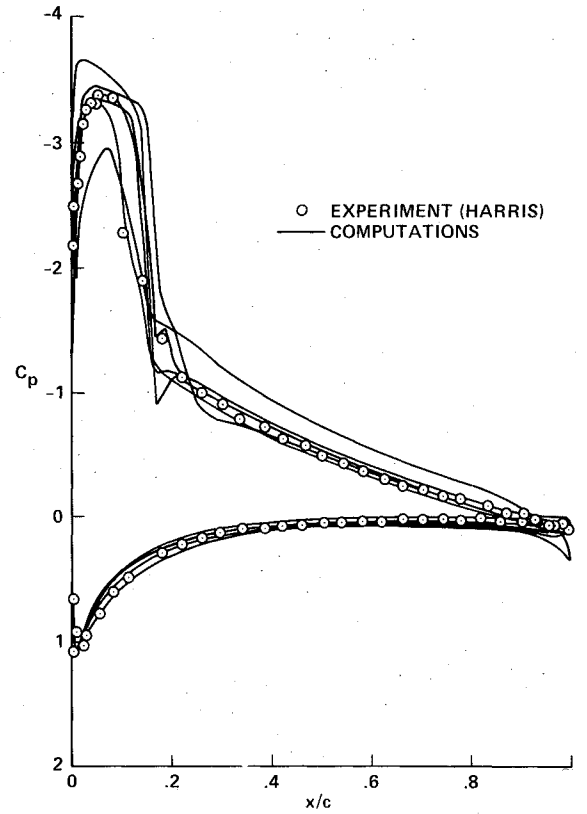

a) Computations utilizing inviscid-plus-boundary-layer methods

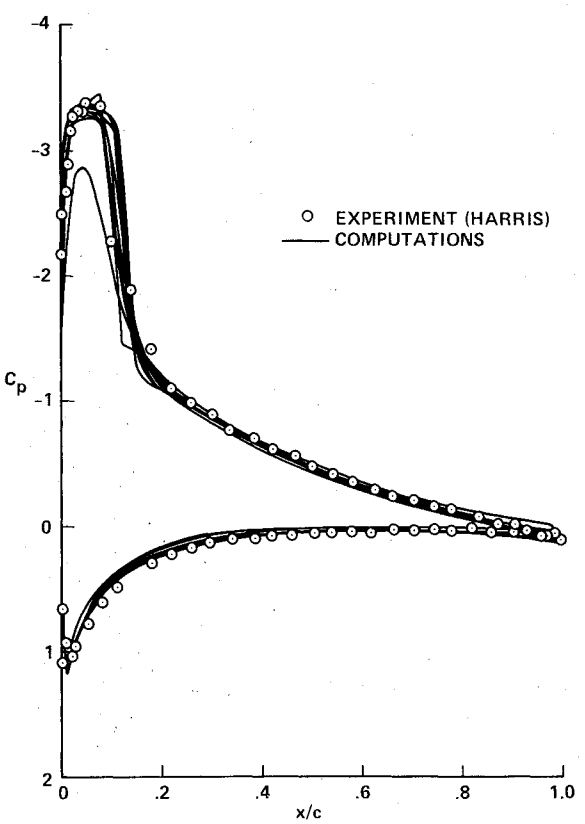

b) Computations utilizing Navier-Stokes methods.

Fig. 2 Comparison of pressure distributions for the NACA 0012 airfoil, $M_\infty = 0.55$, $\alpha = 8.34$ deg (corrected), $Re_c = 9.0 \times 10^6$.

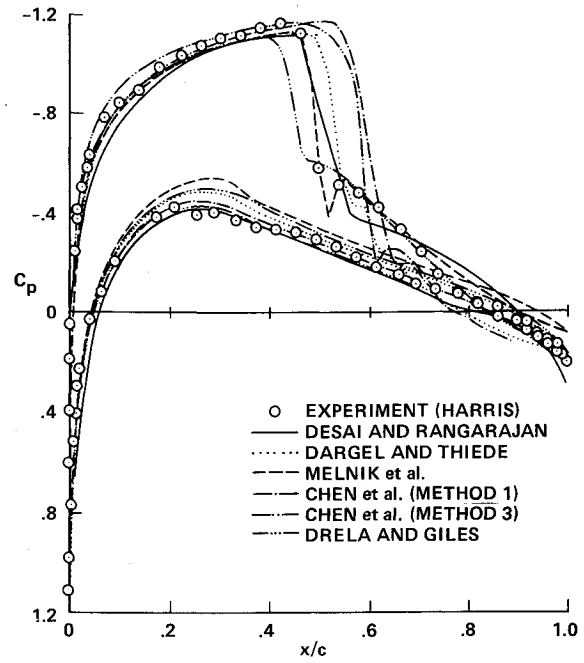

a) Computations utilizing inviscid-plus-boundary-layer methods

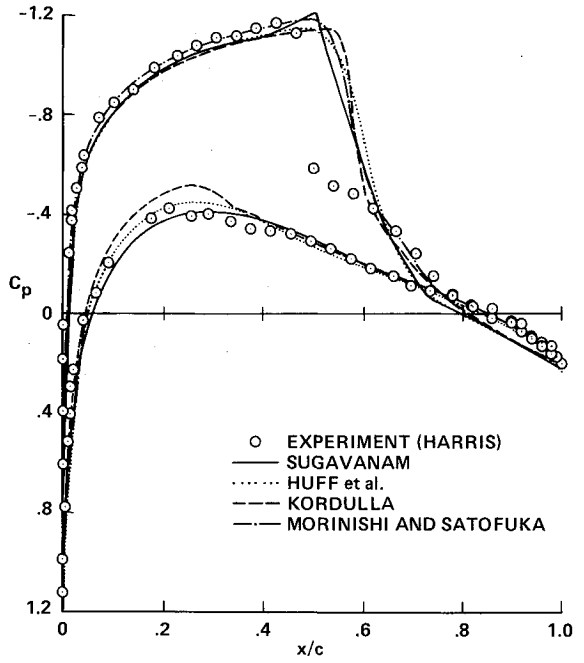

b) Computations utilizing Navier-Stokes methods on coarse grids

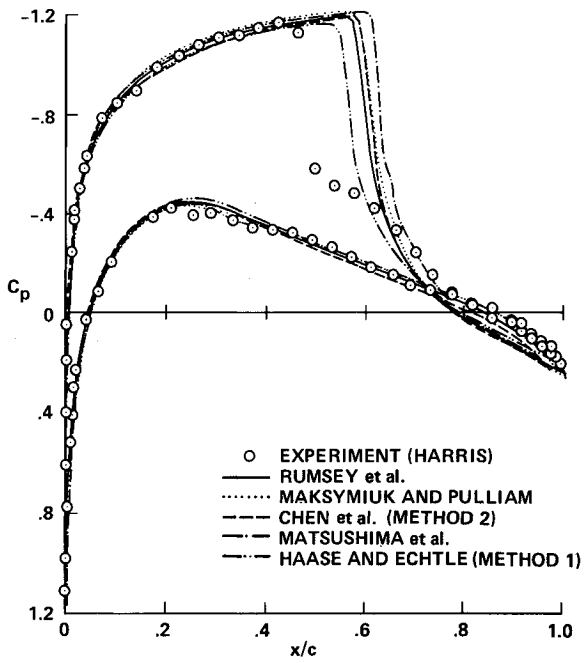

c) Computations utilizing Navier-Stokes methods on fine grids

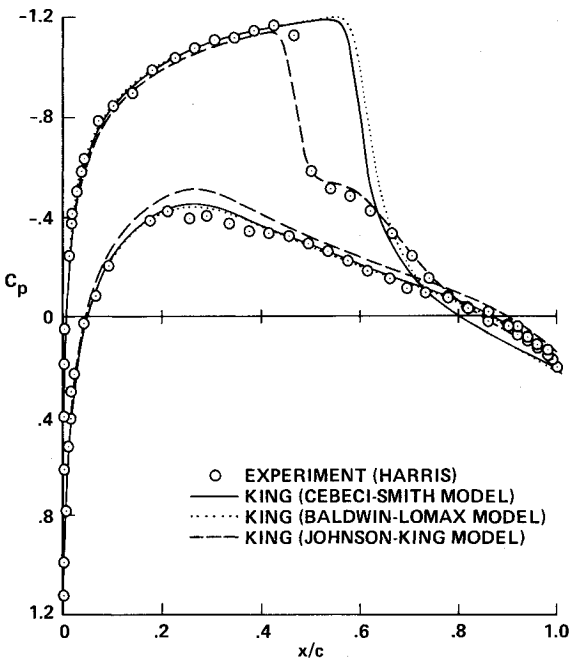

d) Navier-Stokes computations with turbulence model variation due to King[10]

Fig. 3 Comparison of pressure coefficient distributions for the NACA 0012 airfoil, $M_\infty = 0.799$, $\alpha = 2.26$ deg (corrected), $Re_c = 9.0 \times 10^6$.

The computed results for this case are displayed in two different plots (all without labels). Computations utilizing inviscid-plus-boundary-layer methods (six curves) are displayed in Fig. 2a, and computations utilizing Navier-Stokes methods (16 curves) are displayed in Fig. 2b. Both sets of computations are in good agreement with Harris's experimental data. However, the inviscid-plus-boundary-layer results show considerably more scatter for this case than the Navier-Stokes results. Most of the scatter is associated with the solution near the airfoil leading edge on the upper surface, where the large angle of attack causes a rapid expansion followed almost immediately by a shock wave. Perhaps the generally coarser streamwise spacing for the inviscid grids used in the inviscid-plus-boundary-layer methods, which averaged 137 points relative to an average of 243 points for the Navier-Stokes methods, is inadequate to capture the large gradients associated with the inviscid flow at the airfoil leading edge. The two solutions that significantly underpredict the peak $-c_p$ level at the upper-surface leading edge (one result from Fig. 2a and one result from Fig. 2b) are from very coarse-grid calculations and, therefore, tend to support this observation.

Comparisons of pressure coefficient distributions for the third NACA 0012 airfoil case are displayed in Fig. 3. The flow conditions for this case are $M_\infty = 0.799$, $\alpha = 2.26$ deg, and $Re_c = 9 \times 10^6$. Again, the computational angle of attack (2.26 deg) is obtained from the measured angle of attack (2.86 deg) using a linear wind-tunnel-wall correction procedure. For this flowfield, a shock wave exists on the airfoil upper surface at about $x/c = 0.5$, which is strong enough to cause significant boundary-layer separation. This case represents a severe test for all methods. The results are divided into

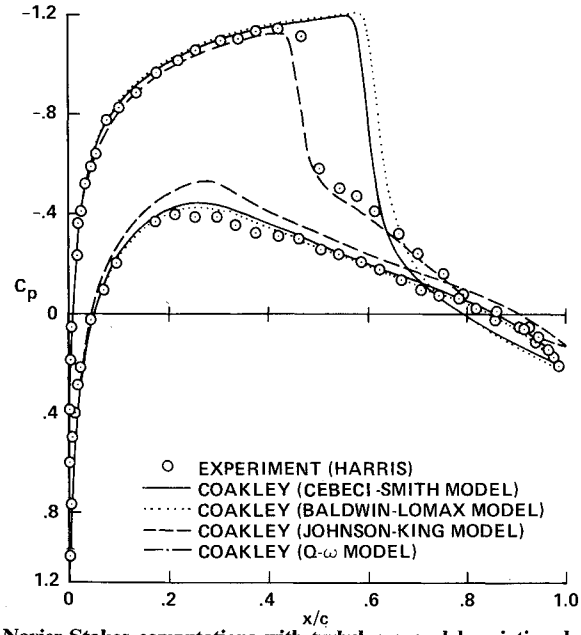

e) Navier-Stokes computations with turbulence model variation due to Coakley [7]

Fig. 3 (continued) Comparison of pressure coefficient distributions for the NACA 0012 airfoil, $M_\infty = 0.799$, $\alpha = 2.26$ deg (corrected), $Re_c = 9.0 \times 10^6$.

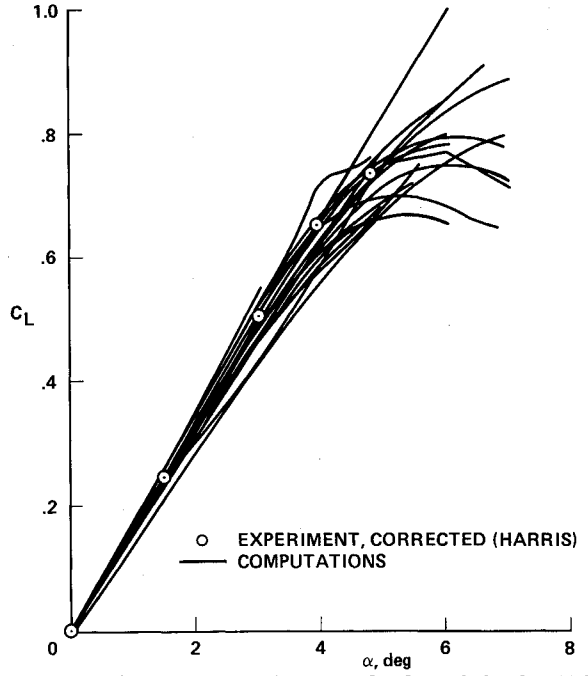

Fig. 4 Comparison of lift coefficient vs angle of attack for the NACA 0012 airfoil, $M_\infty = 0.7$, $Re_c = 9.0 \times 10^6$.

five groups as follows: 1) computations utilizing inviscid-plus-boundary-layer methods (six curves), 2) computations utilizing Navier-Stokes methods on coarse grids (four curves), 3) computations utilizing Navier-Stokes methods on fine grids (five curves), 4) Navier-Stokes computations with turbulence model variation due to King[10] (three curves), and 5) Navier-Stokes computations with turbulence model variation due to Coakley[7] (four curves). The coarse-grid Navier-Stokes results were computed on grids ranging from 127×32 to 193×49, and the fine-grid results ranged from 257×57 to 265×101.

The inviscid-plus-boundary-layer results (Fig. 3a) show a significant amount of scatter, especially at the shock wave and on the lower surface. Nevertheless, several of these methods do a good job in predicting both the position and strength of the shock wave. The coarse-grid Navier-Stokes results shown in Fig. 3b are generally in close agreement with each other but miss both the shock strength and position. The fine-grid Navier-Stokes results (Fig. 3c) are very similar to the coarse-grid results, except the shock is slightly sharper. Thus, grid refinement is not the answer for obtaining good agreement for this case.

The turbulence model used in all but one of the nine Navier-Stokes computations shown in Figs. 3b and 3c was the Baldwin-Lomax[20] model. In Fig. 3d, King[10] has computed results for three different turbulence models, including Baldwin-Lomax, Cebeci-Smith,[21] and the newer Johnson-King[22] model. In Fig. 3e, Coakley[7] has computed results for four different turbulence models, including Baldwin-Lomax, Cebeci-Smith, Johnson-King, and a two-equation model called Q-ω.[23] Note that Q-ω and Cebeci-Smith results are identical and, therefore, are plotted as a single solid line. For the computations in Figs. 3d and 3e, only the turbulence model was allowed to vary; all the other physical and numerical factors were held fixed. The Baldwin-Lomax, Cebeci-Smith, and Q-ω results from both codes produce results that are essentially identical to the other Navier-Stokes results (see Figs. 3b and 3c). The shock is too strong and too far aft on the airfoil. However, the Johnson-King results are in excellent agreement at the shock, accurately predicting both shock position and strength. One drawback associated with the Johnson-King model computations is the underprediction of pressure on the airfoil lower surface. This, of course, will lead to a significant underprediction in lift relative to the experimental value. It is interesting to note that most of the inviscid-plus-boundary-layer results displayed in Fig. 3a, which agree well with the upper-surface shock strength and position, also underpredict the lower-surface pressure distribution.

Figure 4 shows a comparison of 22 C_L vs α curves plotted without labels for the NACA 0012 airfoil at $M_\infty = 0.7$ and $Re_c = 9 \times 10^6$. Experimental results from Harris with wind-tunnel-wall corrections included are also displayed. Most of the computed curves show good agreement with each other and with experiment at lower angles of attack. However, the overall comparison is disappointing at higher angles of attack. The scatter in the maximum lift value is particularly large. The $\alpha = 1.49$ deg experimental point corresponds to the slightly transonic solution shown in Fig. 1, where agreement is generally good. For angles of attack above this point, the flow is more strongly transonic and eventually separates. In addition, several authors reported convergence difficulties or solution unsteadiness at these higher angles of attack. This may be a contributing factor to the large amount of scatter in the maximum C_L.

Drag polar comparisons are displayed in Fig. 5 for the NACA 0012 airfoil at $M_\infty = 0.7$ and $Re_c = 9 \times 10^6$. As before, this set of comparisons is broken into several parts, with the experimental results of Harris included in each part for comparison. For $C_L \sim 0.2$ and lower, the flowfield is subsonic. Drag values below this point correspond to pressure-plus-skin-friction drag, and values above this point have, in addition, a wave-drag component. Since the pressure comparisons shown in Fig. 1 are all in good agreement, any disagreement in subcritical drag shown in Fig. 5 is probably due to disagreements in the skin-friction-drag component. However, since the pressure integration for drag can be quite sensitive, this assertion should be studied in more detail by examining computed drag-component results.

Turbulence model variation has an effect on the drag polar, as shown in Figs. 5e and 5f. For both figures, the newer Johnson-King turbulence model results overpredict the drag in comparison with experiment for the higher lift values, while the older models yield reasonable agreement. This trend is rather puzzling, since the Johnson-King model yielded the best pressure distribution through the shock wave for the

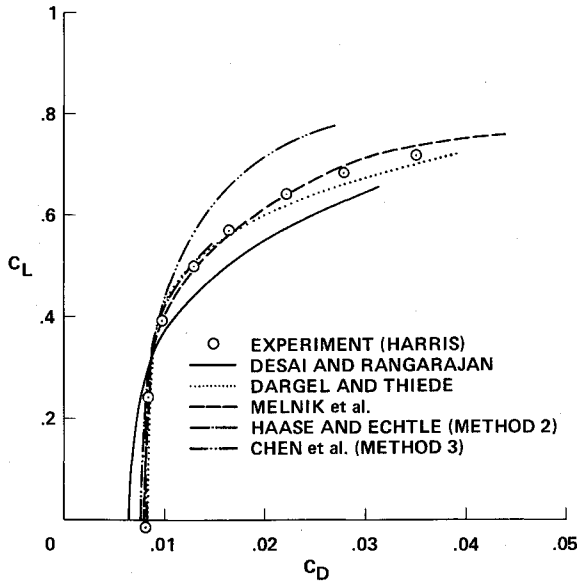

a) Computations utilizing potential-plus-boundary-layer methods

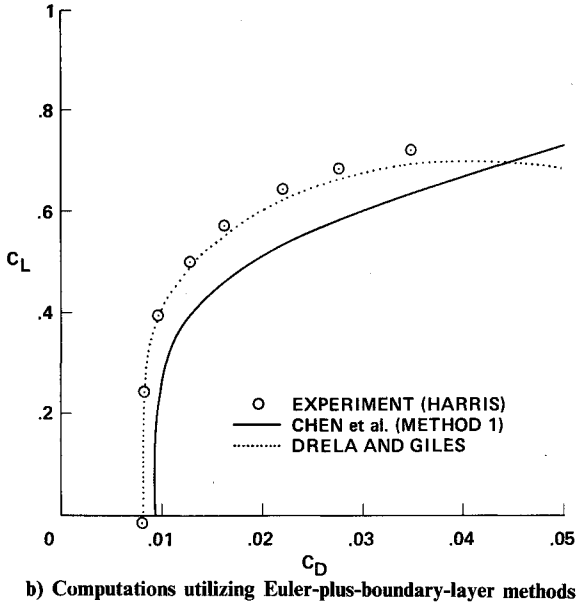

b) Computations utilizing Euler-plus-boundary-layer methods

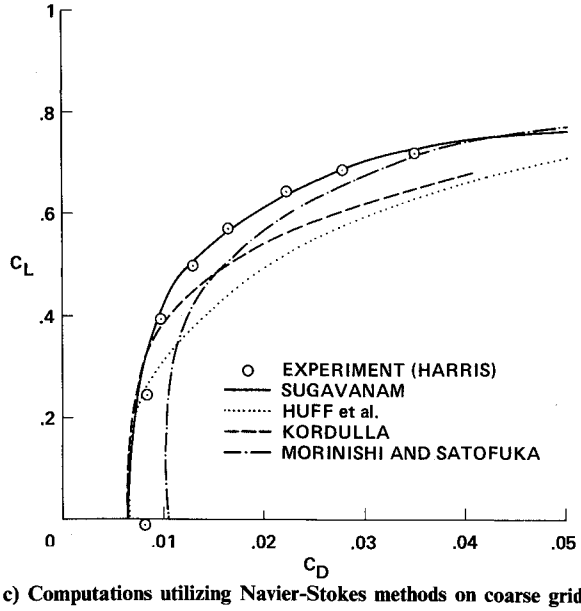

c) Computations utilizing Navier-Stokes methods on coarse grids

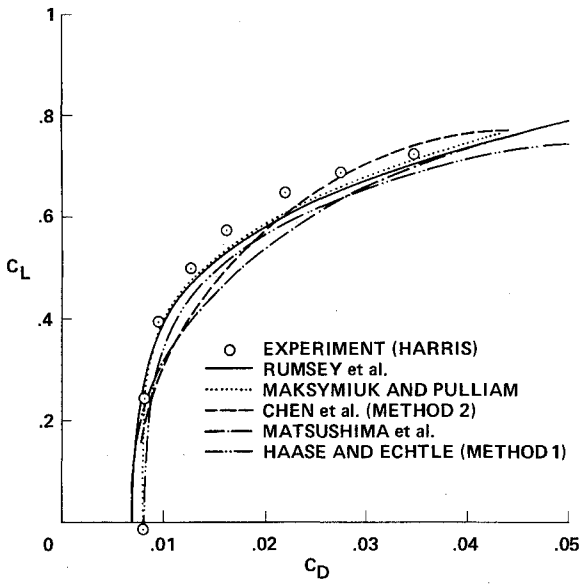

d) Computations utilizing Navier-Stokes methods on fine grids

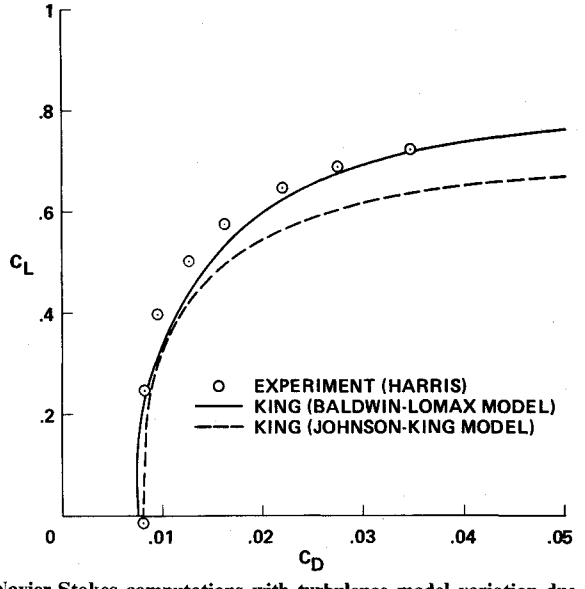

e) Navier-Stokes computations with turbulence model variation due to King[10]

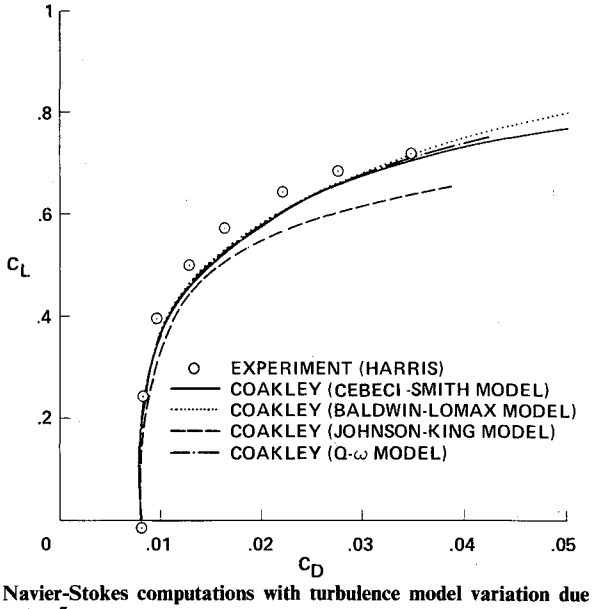

f) Navier-Stokes computations with turbulence model variation due to Coakley[7]

Fig. 5 Comparison of lift vs drag polars for tne NACA 0012 airfoil, $M_\infty = 0.7$, $Re_c = 9.0 \times 10^6$.

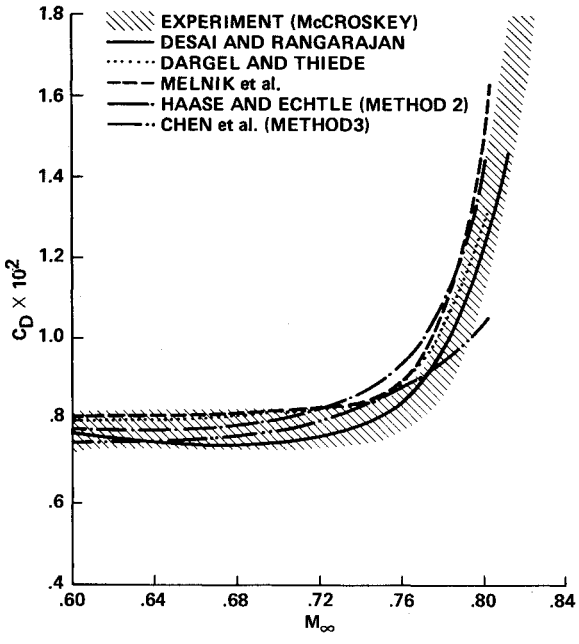

a) Computations utilizing potential-plus-boundary-layer methods

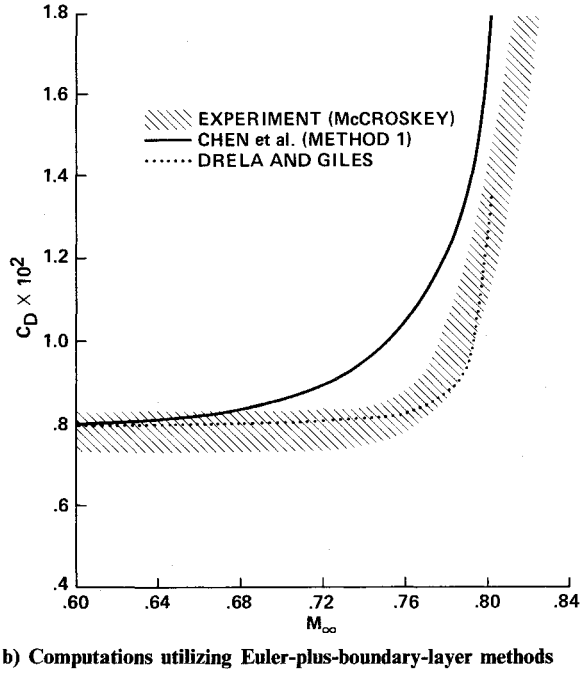

b) Computations utilizing Euler-plus-boundary-layer methods

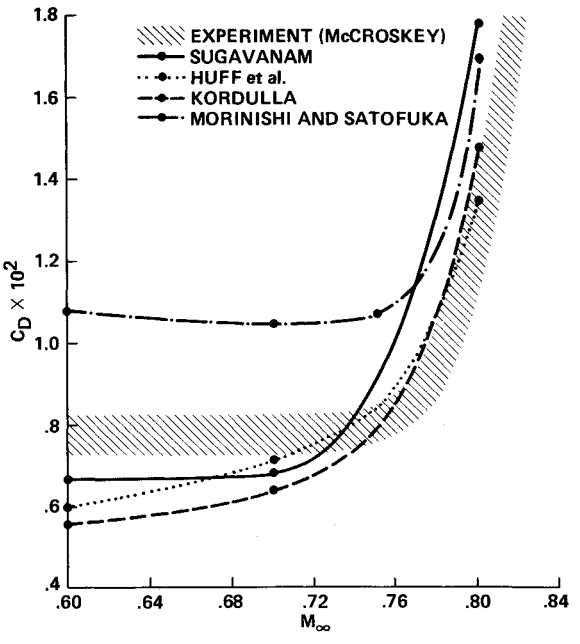

c) Computations utilizing Navier-Stokes methods on coarse grids

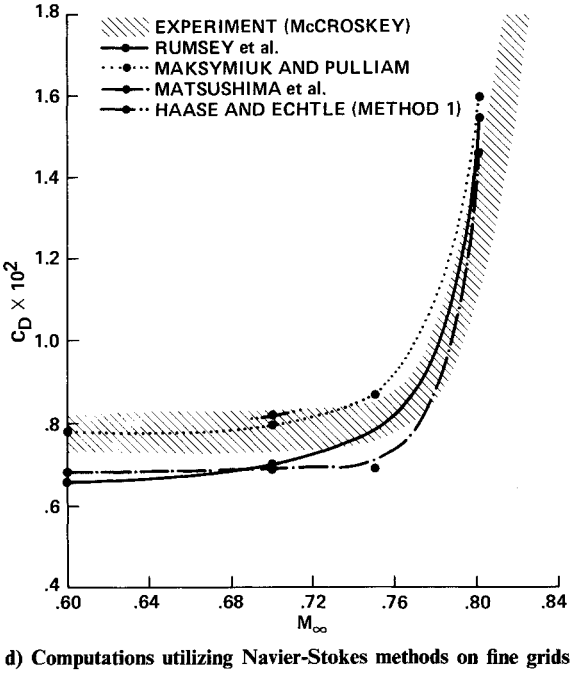

d) Computations utilizing Navier-Stokes methods on fine grids

Fig. 6 Comparison of computed and measured transonic drag-rise characteristics for the NACA 0012 airfoil, $\alpha = 0$ deg, $Re_c = 9.0 \times 10^6$.

strongly separated case presented in Fig. 3. Perhaps the reason for poor drag polar agreement is associated with the underprediction of lower-surface pressure as predicted by the Johnson-King model in Figs. 3d and 3e. This would lower the lift, and if the drag is unaffected, produce the situation observed in Figs. 5e and 5f. However, several of the inviscid-plus-boundary-layer results presented in Figs. 5a and 5b also exhibit the same underprediction of pressure but produce good drag polar results. This general area of drag prediction should be the subject of additional study.

Transonic drag-rise characteristics for the NACA 0012 airfoil at zero-lift conditions are displayed in Fig. 6. This set of comparisons is also broken into several parts and compared with a range of experimental data compiled by McCroskey.[24] All computations were performed at a Reynolds number based on airfoil chord of 9 million. The turbulent boundary layer was numerically "tripped" at $x/c = 0.05$ for those methods with trip or transition modeling and at the airfoil leading edge for those methods without. Each numerical curve shown in Fig. 6 is displayed with the computational points used to establish that curve (shown as solid circular symbols) when these points were available and when a small number of points (3 or 4) were used to establish the entire curve.

The range of experimental data displayed in Fig. 6 was established by looking at a large number of experiments (approximately 50). The six "best" sets of data, including Harris,[19] were selected, adjusted for Reynolds number effects, and plotted in Fig. 6 as a cross-hatched region. The different sets of experimental data, the selection process, and the Reynolds number adjustment procedure are described in McCroskey.[25] For this adjusted set of data, at a freestream Mach number of 0.7, the experimental drag value ranges from

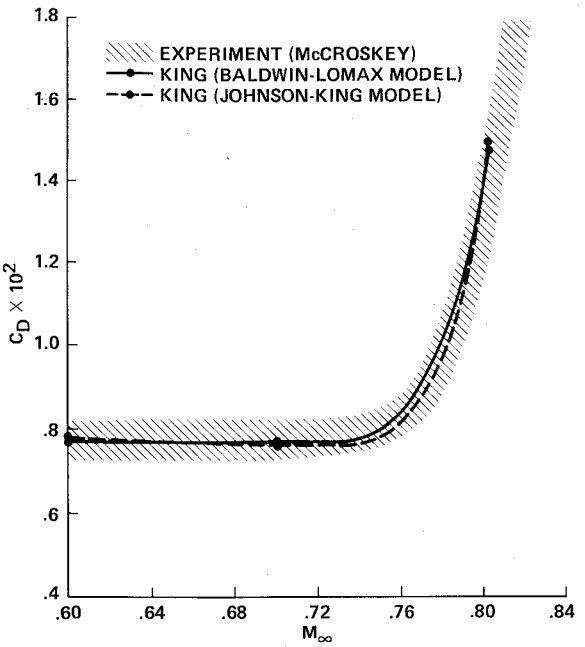

e) Navier-Stokes computations with turbulence model variation due to King[10]

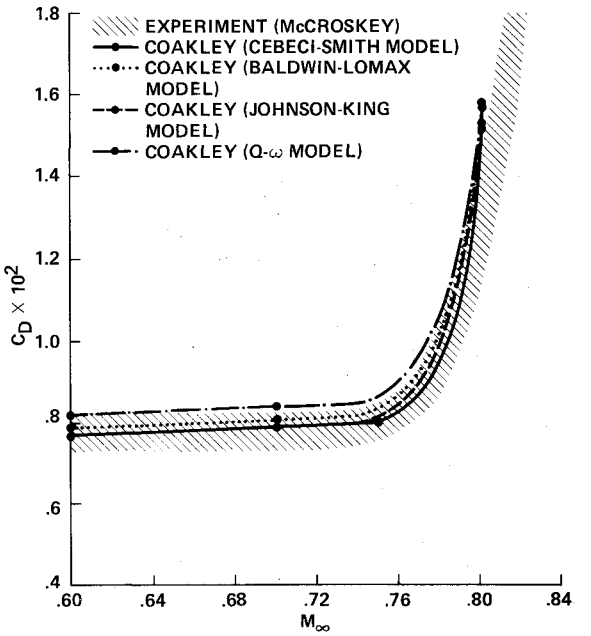

f) Navier-Stokes computations with turbulence model variation due to Coakley.[7]

Fig. 6 (continued) Comparison of computed and measured transonic drag-rise characteristics for the NACA 0012 airfoil, $\alpha = 0$ deg, $Re_c = 9.0 \times 10^6$.

about 73–83 counts. For reference, Harris's highest Reynolds number tripped data produced a drag of about 75 counts.

The inviscid-plus-boundary-layer computations shown in Figs. 6a and 6b generally agree well with each other and with the experimental range of results. The drag-divergence Mach number is difficult to ascertain from some methods, especially the two Euler-plus-boundary-layer results shown in Fig. 6b. The scatter associated with the coarse-grid Navier-Stokes result (Fig. 6c) is quite large relative to the other computational and experimental results, especially at the subsonic Mach numbers, and suggests that the boundary-layer grid refinement, or perhaps grid clustering, is a key parameter for drag calculations. Figures 6e and 6f show the effect of turbulence model variation on the drag-rise characteristics of the NACA 0012 airfoil. Except for relatively small variations in subsonic drag levels, there is virtually no variation in drag rise due to the turbulence models tested for this case.

Figure 7 shows computations (3 curves) compared with a range of experimental data, again compiled by McCroskey,[24] for the lift-curve slope ($dC_L/d\alpha$) plotted vs freestream Mach number. Values for $dC_L/d\alpha$ were obtained by computing the lift at $\alpha = 1.0$ deg. The units on $dC_L/d\alpha$ are therefore $(\text{deg})^{-1}$. This particular curve is significant because of its sensitivity to shock wave position and shock/boundary-layer interaction. The three computed results are in good agreement with the experimental range at lower freestream Mach numbers but deviate quickly. The single inviscid-plus-boundary-layer result starts deviation at about the drag-divergence Mach number. The two Navier-Stokes results qualitatively follow most of the experimental trends, including the severe shock-induced lift loss in the range $0.85 \le M_\infty \le 0.90$, but miss the appropriate levels, especially the minimum value of $dC_L/d\alpha$ at $M_\infty = 0.88$.

RAE 2822 Airfoil Results

The next series of comparisons is for the RAE 2822 airfoil, which has been tested extensively by Cook et al.[26] This airfoil is a supercritical airfoil with a significant amount of aft camber. It is defined by a series of airfoil coordinates that are given in Refs. 26 and 17. The experimental data base given in Ref. 26 is quite extensive, consisting of surface pressures, skin friction, boundary-layer displacement thickness, and boundary-layer velocity profiles. However, unlike the NACA 0012 airfoil, only one experiment is available, and the experimental accuracy is unknown.

Computed pressure coefficient distributions without labels (19 curves) are compared with each other and experiment in Fig. 8 for the RAE 2822 airfoil at $M_\infty = 0.725$, $\alpha = 2.92$ deg, and $Re_c = 6.5 \times 10^6$ (case 6 in Ref. 26). The experimental transition location for this case was fixed at $x/c = 0.03$. For this calculation, the various authors used a variety of corrections on Mach number and angle of attack. The angle of attack corrections will be tabulated along with force coefficients for this case in a subsequent section. For additional details about these corrections, the interested reader is referred to the individual publications. As can be seen from Fig. 8, all results are in generally good agreement, with the largest discrepancies occurring at the shock wave.

Computed skin-friction distributions from the upper surface of the RAE 2822 airfoil for the case just presented are compared in Fig. 9. These skin-friction values are referenced to the boundary-layer edge dynamic pressure. The results indicate an attached solution even through the shock wave. Generally, the computed results are in good agreement with experiment, with exceptions near the leading edge, where the skin-friction quantity is difficult to define or compute, and downstream of the shock wave. Since the skin friction is a derivative quantity, and since it depends on many numerical details, including boundary-layer grid clustering, smoothing, y^+ wall value, etc., it is appropriate to assume that skin friction will be less accurate than a quantity that is directly computed or measured, e.g., pressure or velocity. Thus, the level of skin-friction scatter for this case is deemed acceptable or (at least) within the range of what should be expected with today's CFD technology.

A sample boundary-layer profile from the RAE 2822 airfoil solution just described is displayed in Fig. 10. This profile is taken from the upper-surface solution at $x/c = 0.95$. Computed results from six methods are compared with experiment. The pressure agreement between computations and experiment at this location (see Fig. 8) is excellent. However, the skin-friction agreement between computations and experiment at this location is only fair (see Fig. 9). Nevertheless, the velocity profile agreement seems to be good.

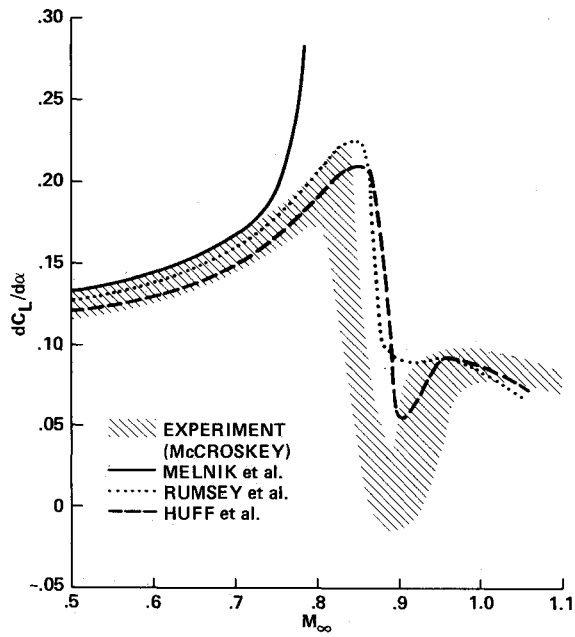

Fig. 7 Comparison of computed and measured results for the lift-curve slope as a function of the freestream Mach number, NACA 0012 airfoil.

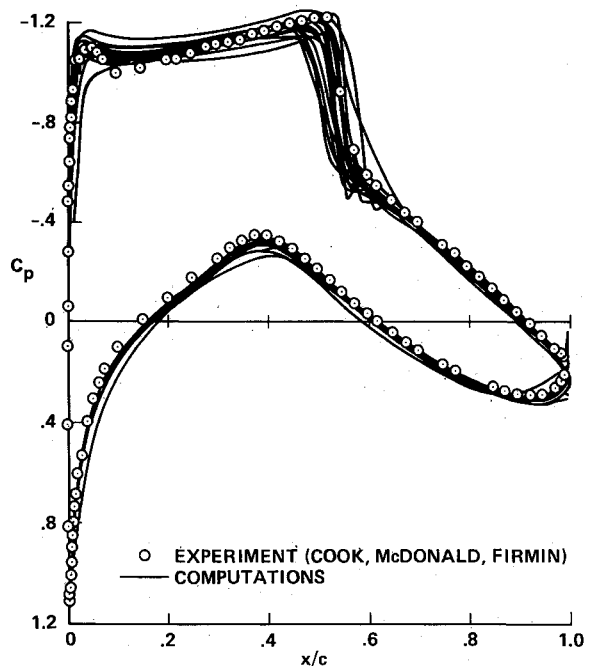

Fig. 8 Comparison of pressure coefficient distributions for the RAE 2822 airfoil, $M_\infty = 0.725$, $\alpha = 2.92$ deg (uncorrected), $Re_c = 6.5 \times 10^6$.

The second RAE 2822 airfoil case presented corresponds to case 10 of Ref. 26, $M_\infty = 0.75$, $\alpha = 3.19$ deg, and $Re_c = 6.2 \times 10^6$. This case is one of the most difficult RAE 2822 cases presented in Ref. 26, as the shock wave causes a significant amount of boundary-layer separation. Computed pressure coefficient distributions are compared with the experiment in Fig. 11. As before, these results are divided into several parts, each with experimental comparisons. The inviscid-plus-boundary-layer results shown in Fig. 11a are generally in good agreement with experiment. Some scatter in the pressure results occurs aft of the shock wave on the airfoil upper surface. The coarse- and fine-grid Navier-Stokes results presented in Figs. 11b and 11c show a relatively small amount

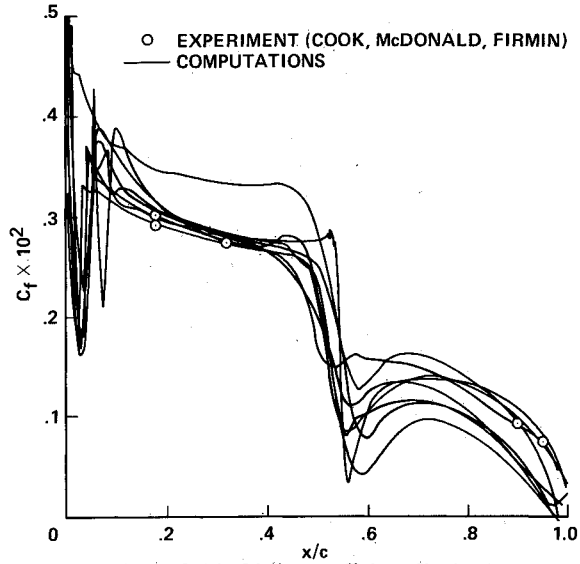

Fig. 9 Comparison of skin-friction coefficient distributions from the RAE 2822 airfoil upper surface, $M_\infty = 0.725$, $\alpha = 2.92$ deg (uncorrected), $Re_c = 6.5 \times 10^6$.

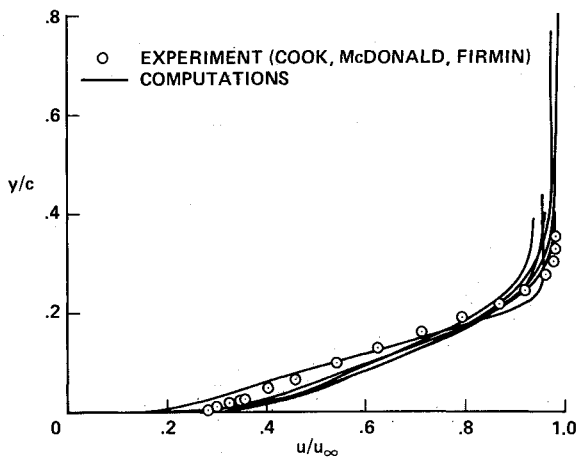

Fig. 10 Velocity profile comparisons from the RAE 2822 airfoil upper surface at $x/c = 0.95$, $M_\infty = 0.725$, $\alpha = 2.92$ deg (uncorrected), $Re_c = 6.5 \times 10^6$.

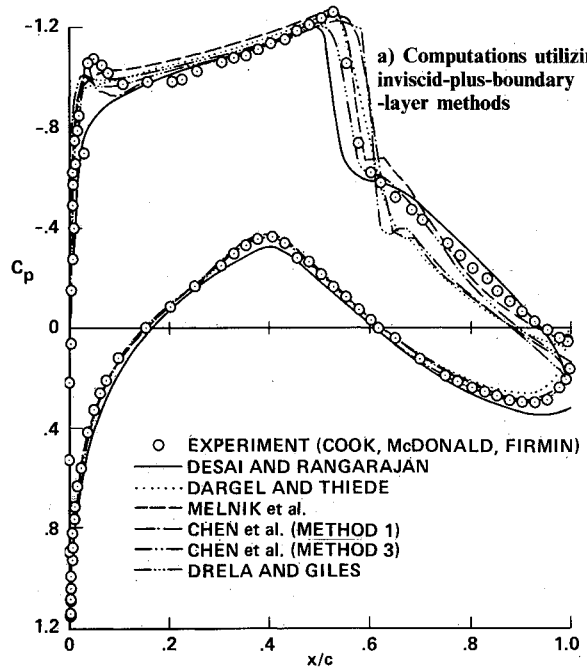

Fig. 11 Comparison of pressure coefficient distributions for the RAE 2822 airfoil, $M_\infty = 0.75$ (uncorrected), $\alpha = 3.19$ deg (uncorrected), $Re_c = 6.2 \times 10^6$.

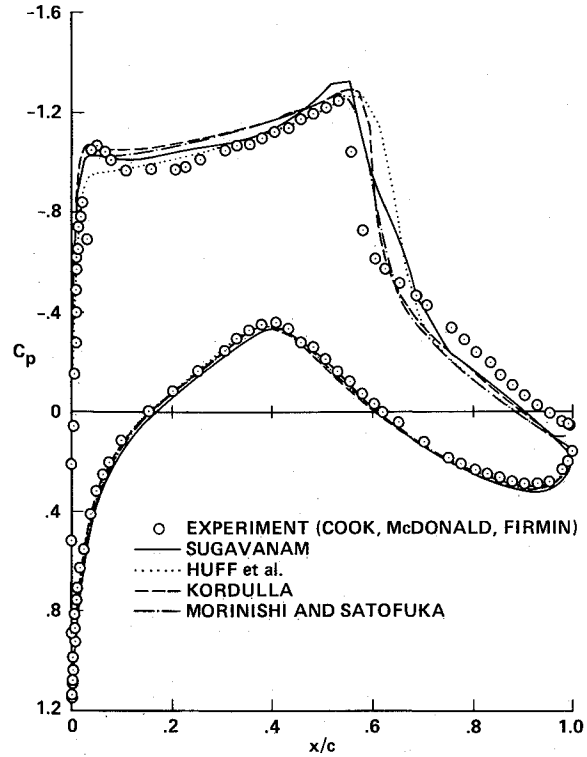

b) Computations utilizing Navier-Stokes methods on coarse grids

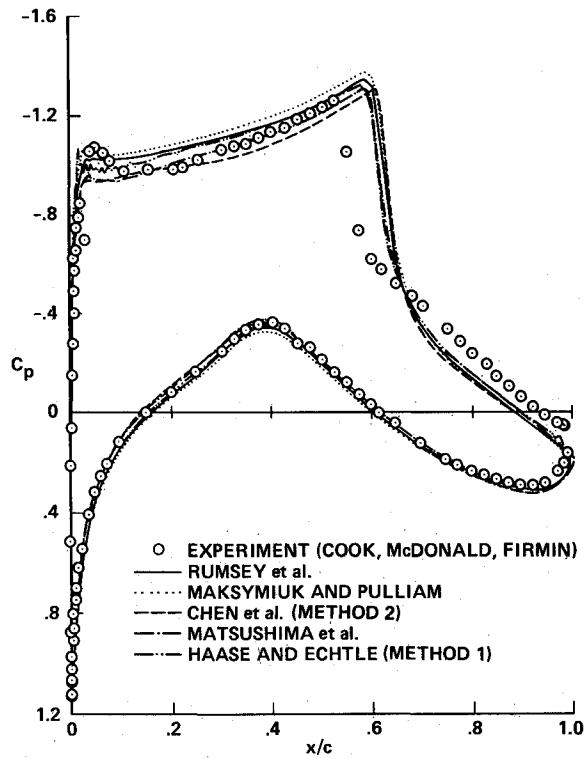

c) Computations utilizing Navier-Stokes methods on fine grids

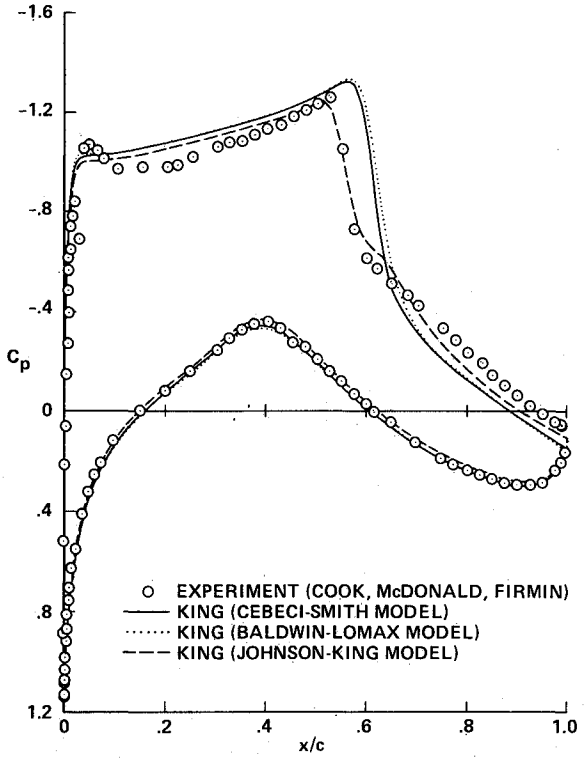

d) Navier-Stokes computations with turbulence model variation due to King[10]

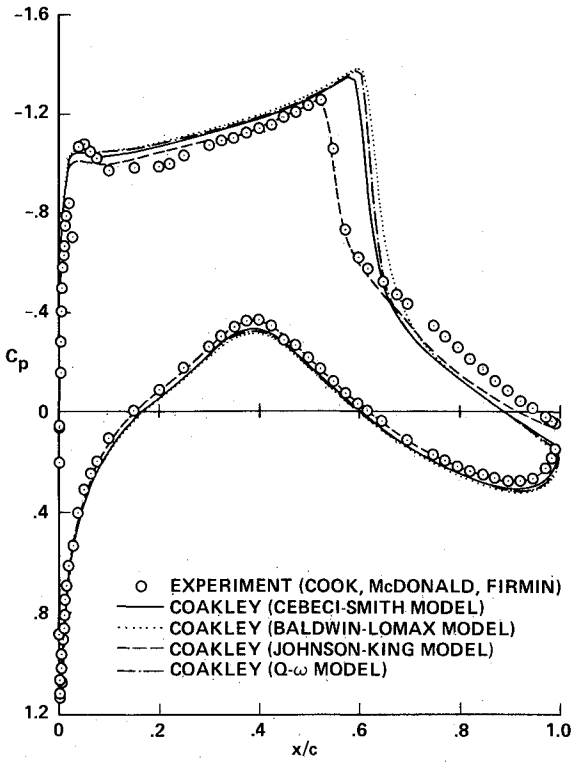

e) Navier-Stokes computations with turbulence model variation due to Coakley[7]

Fig 11 (continued) Comparison of pressure coefficient distributions for the RAE 2822 airfoil, $M_\infty = 0.75$ (uncorrected), $\alpha = 3.19$ deg (uncorrected), $Re_c = 6.2 \times 10^6$.

of scatter and good agreement with experiment everywhere, except at and aft of the shock wave. The Navier-Stokes shock position is consistently too far downstream, and the strength is too large. The coarse-grid results (Fig. 11b) show a little more scatter at the shock and are slightly more smeared than the fine-grid results (Fig. 11c). However, both sets of results are essentially in agreement.

The general agreement between all the Navier-Stokes results indicates a relatively low amount of numerical error from method to method. The uniform discrepancy with experiment at the shock wave is an indication of a consistent error in the physical model, probably the turbulence model. All Navier-Stokes results shown in Figs. 11b and 11c use the Baldwin-Lomax or similar algebraic turbulence model. This

model is known to overpredict shock strength and position for separated flow cases. The pressure distribution comparisons already presented in Figs. 3b and 3c are additional examples of this behavior.

Figures 11d and 11e show the effect of turbulence model on the pressure distribution for the Navier-Stokes approach. As with the NACA 0012 airfoil results shown in Figs. 3d and 3e, the only formulational variations in each of these two sets of results is the turbulence model. Four turbulence models are utilized: 1) Cebeci-Smith,[20] 2) Baldwin-Lomax,[19] 3) Johnson-King,[21] and 4) the two-equation Q-ω model.[22] Only the Johnson-King model results produce good agreement with experiment everywhere, except for a slight disagreement downstream of the shock wave on the airfoil upper surface. All the other results are in close agreement with the Navier-Stokes results of Figs. 11b and 11c. Note that the lower-surface pressure levels predicted by all methods (Figs. 11a–11e) for this RAE 2822 airfoil case are in close agreement with experiment. This is in direct contrast to the separated NACA 0012 airfoil results shown in Fig. 3. Although this behavior may be partly due to differences in the basic flow physics associated with the NACA 0012 and RAE 2822 airfoils, a complete explanation of this behavior is unknown.

Computed boundary-layer displacement thickness distributions for the case 10 RAE 2822 airfoil solutions presented in the previous figure are compared with experiment in Fig. 12. The displacement thickness is normalized by airfoil chord, and only upper-surface distributions are presented. As before, these curves are displayed in several parts. Agreement upstream of the shock wave is excellent for all computational and experimental results. Downstream of the shock wave, a large variation occurs for all method categories. The methods that generally had good pressure agreement at the shock wave tend to have better agreement with the experimental displacement thickness through and aft of the shock wave. Methods that predicted shocks too strong and too far aft generally underpredict the displacement thickness downstream of the shock. It is interesting to note that none of the computational

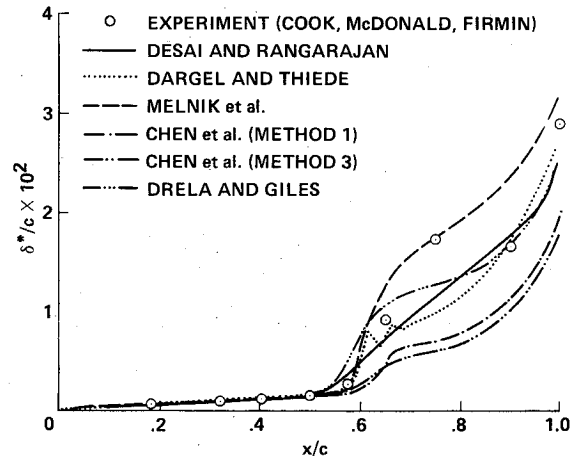

a) Computations utilizing inviscid-plus-boundary-layer methods

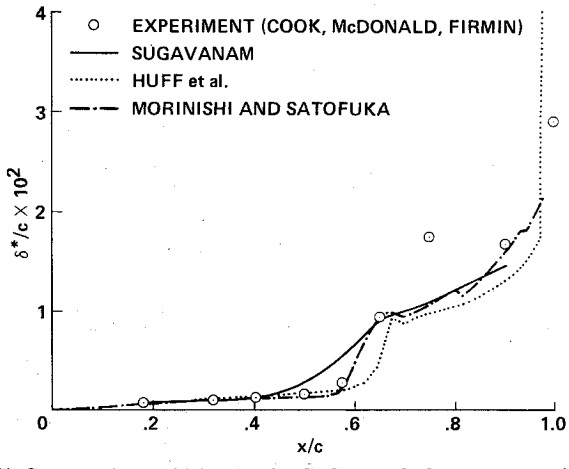

b) Computations utilizing Navier-Stokes methods on coarse grids

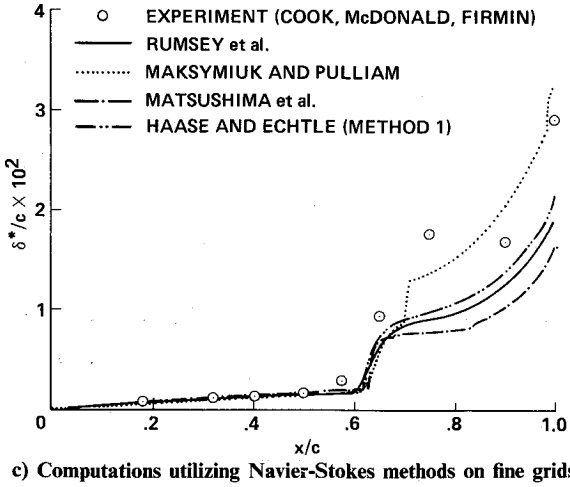

c) Computations utilizing Navier-Stokes methods on fine grids

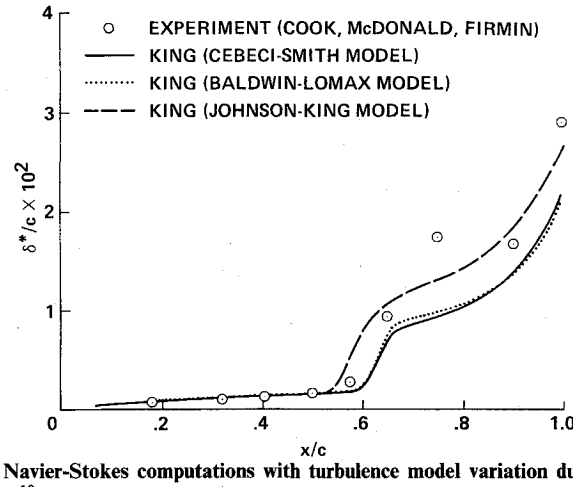

d) Navier-Stokes computations with turbulence model variation due to King[10]

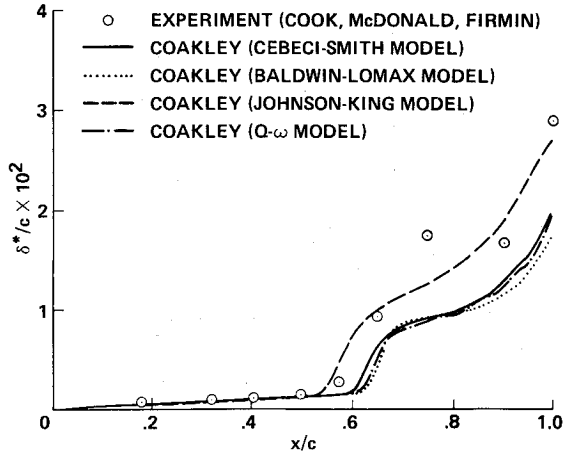

e) Navier-Stokes computations with turbulence model variation due to Coakley[7]

Fig. 12 Comparison of upper-surface boundary-layer displacement thickness for the RAE 2822, $M_\infty = 0.75$ (uncorrected), $\alpha = 3.19$ deg (uncorrected), $Re_c = 6.2 \times 10^6$.

methods predicts the decreasing δ^*/c trend, with a local minimum that occurs at $x/c = 0.8$ in the experimental data.

The computed upper-surface skin-friction distributions for the case 10 RAE 2822 airfoil are compared with experiment in Fig. 13. As in the previous two figures, this set of results is displayed in several parts, with all skin-friction values referenced to boundary-layer edge conditions. For this case, most of the methods predict flow separation at the shock wave. The reattachment point varies dramatically from just downstream of separation all the way to the airfoil trailing edge.

The results shown in Fig. 13a for the inviscid-plus-boundary-layer methods show the most consistency with each other and generally good agreement with experimental data. One result in Fig. 13a, which predicts attached flow over the entire airfoil, does not agree well with the other results downstream of the shock wave. This result was computed using a coarse inviscid grid, which is perhaps the reason for the observed disagreement. The Navier-Stokes results of Fig. 13b show more scatter than most of the inviscid-plus-boundary-layer results but still generally agree with experiment. The Navier-Stokes results with turbulence model variation (Figs. 13c and 13d) show skin-friction differences that are similar to those of Fig. 13a. Most of the solutions utilizing the simple turbulence models, including Cebeci-

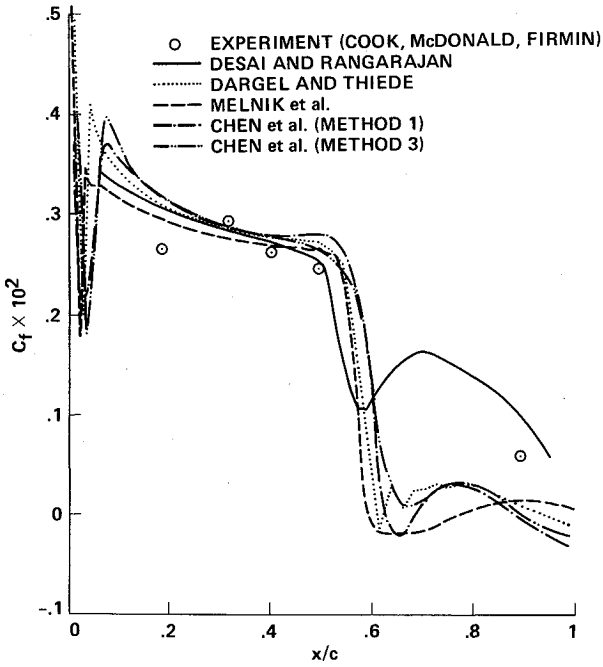

a) Computations utilizing inviscid-plus-boundary-layer methods

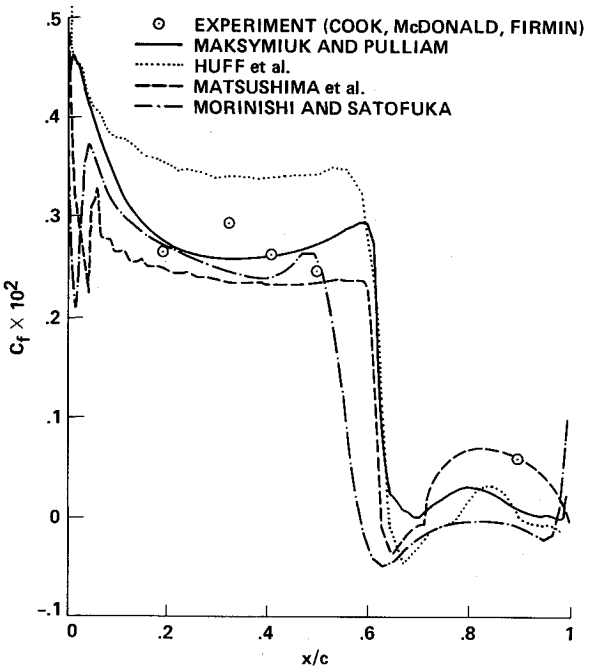

b) Computations utilizing Navier-Stokes methods

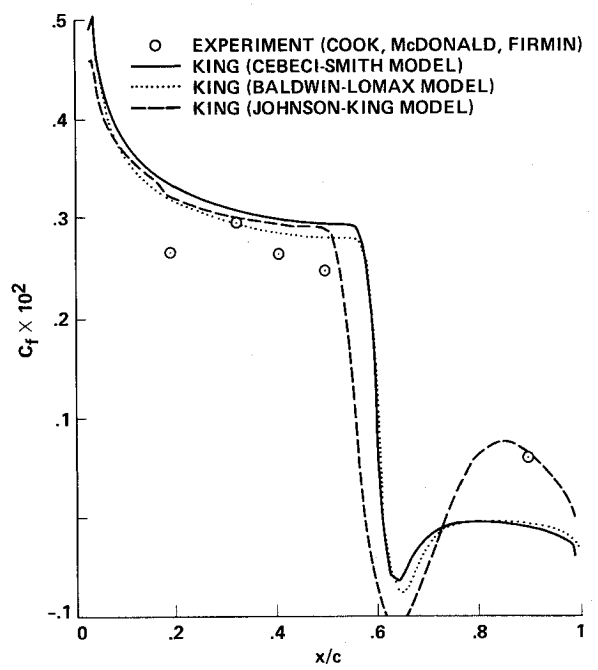

c) Navier-Stokes computations with turbulence model variation due to King[10]

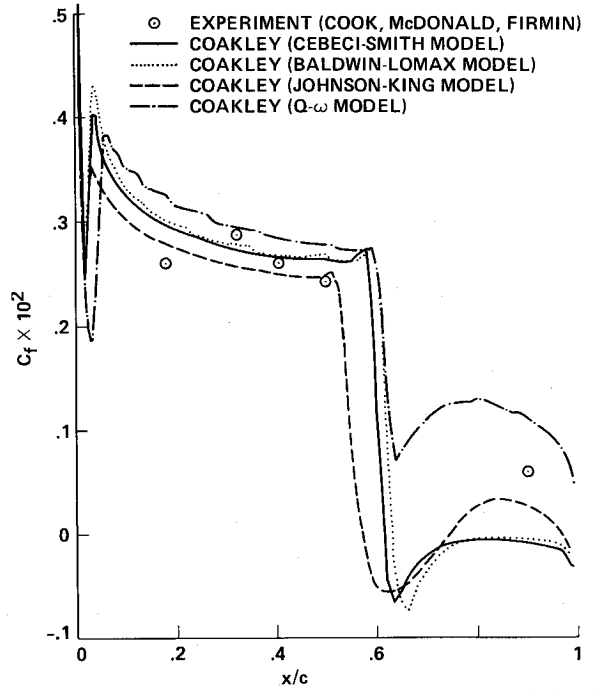

d) Navier-Stokes computations with turbulence model variation due to Coakley[7]

Fig. 13 Comparison of skin-friction coefficient distributions for the RAE 2822 airfoil upper surface, $M_\infty = 0.75$ (uncorrected), $\alpha = 3.19$ deg (uncorrected), $Re_c = 6.2 \times 10^6$.

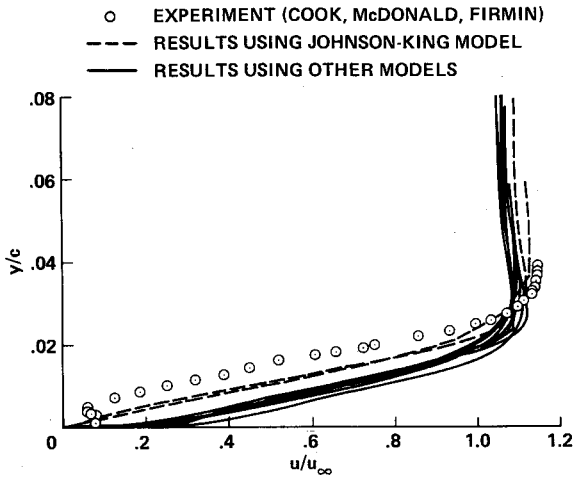

Fig. 14 Velocity profile comparisons from the RAE 2822 airfoil upper surface at $x/c = 0.75$, $M_\infty = 0.75$ (uncorrected), $\alpha = 3.19$ deg (uncorrected), $Re_c = 6.2 \times 10^6$.

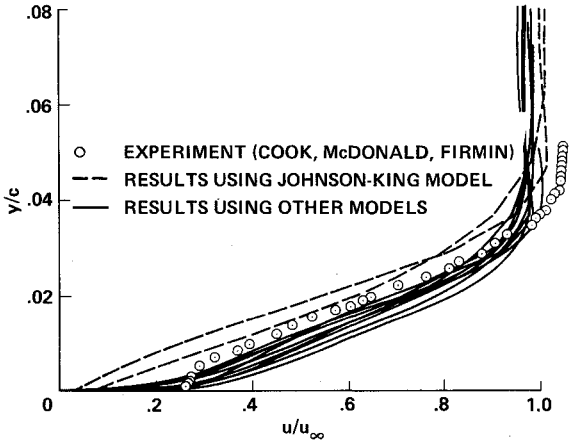

Fig. 15 Velocity profile comparisons from the RAE 2822 airfoil upper surface at $x/c = 0.9$, $M_\infty = 0.75$ (uncorrected), $\alpha = 3.19$ deg (uncorrected), $Re_c = 6.2 \times 10^6$.

Smith, Baldwin-Lomax, and Johnson-King, predict separation at the shock and reattachment that varies widely. Only the more complex two-equation Q-ω model predicts attached flow along the entire airfoil upper surface. This suggests that many factors, including numerical aspects, such as artificial dissipation, grid resolution, surface grid clustering, etc., and physical modeling aspects, such as turbulence modeling, affect skin-friction distributions. Overall, the present computational methods, although having difficulties with separated flow, do a reasonable job of predicting skin friction.

In an attempt to understand some of the more detailed flow physics associated with the boundary layer, two sets of velocity boundary-layer profiles from the case 10 RAE 2822 airfoil[26] are compared in Figs. 14 and 15 with each other and experiment. Figure 14 shows results from the upper-surface boundary layer taken at $x/c = 0.75$, which is generally in the vicinity of reattachment. Figure 15 shows the same set of results for $x/c = 0.95$, which is generally in the attached flow region near the trailing edge. Because the Johnson-King turbulence model results of King[10] and Coakley[7] are so different from the other profiles, these results are indicated with dashed lines in both Figs. 14 and 15. All other results are drawn as solid lines. With the exception of one Euler-plus-boundary layer method, all methods used to produce curves in Figs. 14 and 15 are from Navier-Stokes methods. No results are included from the popular momentum integral boundary-layer methods because of the lack of an easily defined velocity

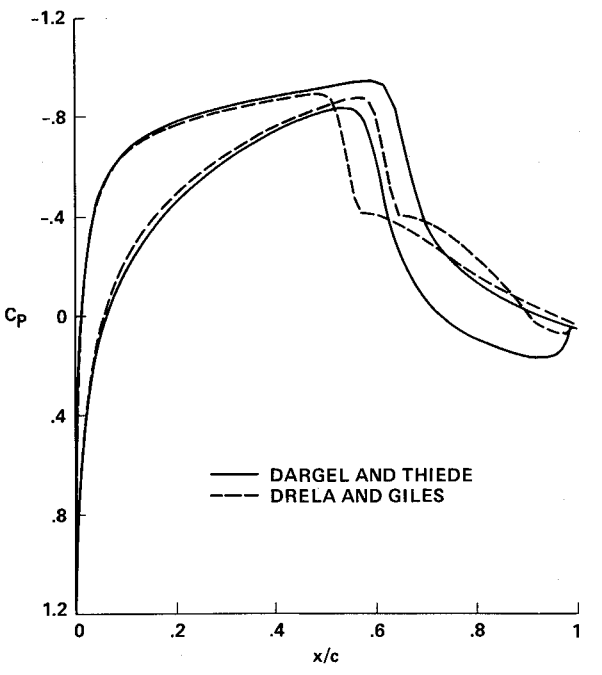

a) Computations utilizing inviscid-plus-boundary-layer methods

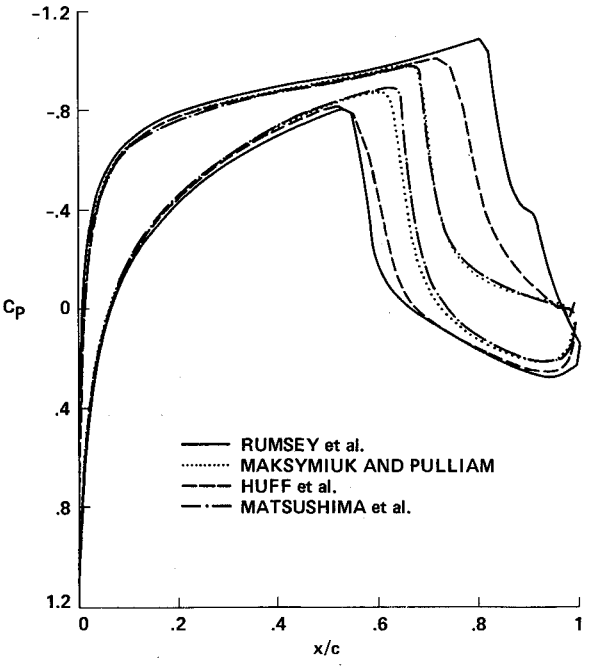

b) Computations utilizing Navier-Stokes methods

Fig. 16 Comparison of pressure coefficient distributions for the Jones airfoil, $M = 0.85$, $\alpha = 2.0$ deg, $Re_c = 9.0 \times 10^6$.

profile in this approach. In Fig. 14, the experimental velocity profile is less full than all of the computed profiles, most of which use the Baldwin-Lomax turbulence model. The two Johnson-King model results approximately split the difference between experiment and the other computed results, indicating that this model is "moving in the right direction." The velocity profile comparison in Fig. 15 is somewhat different, with the experimental data splitting the difference between the two different types of computations. Thus, with respect to Figs. 14 and 15, the Johnson-King model is the best turbulence model, but there is still considerable room for improvement.

One last point regarding experimental/computational comparisons should be made. Although the physical modeling

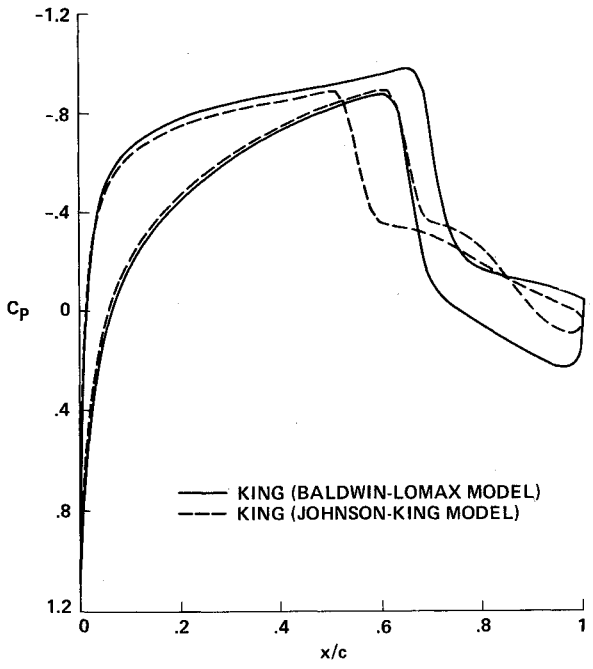

c) Navier-Stokes computations with turbulence model variation due to King[10]

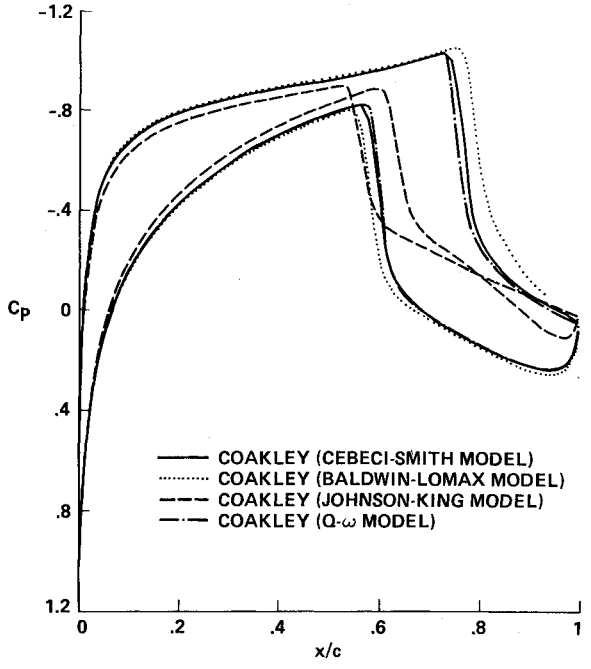

d) Navier-Stokes computations with turbulence model variation due to Coakley[7]

Fig. 16 (continued) Comparison of pressure coefficient distributions for the Jones airfoil, $M = 0.85$, $\alpha = 2.0$ deg, $Re_c = 9.0 \times 10^6$.

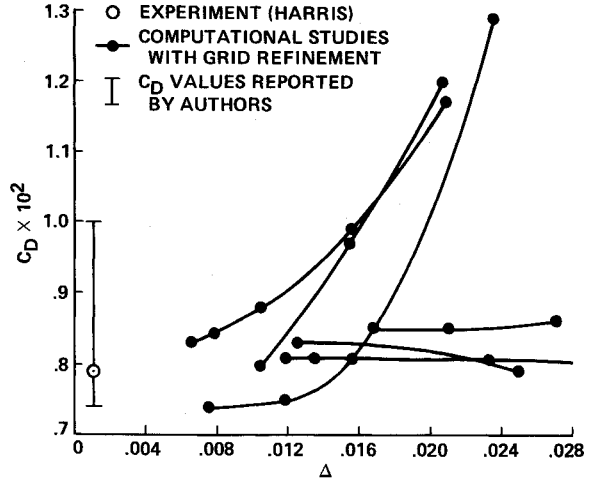

Fig. 17 Computed drag coefficient vs average grid spacing on the airfoil upper surface (Δ) for the NACA 0012 airfoil (grid refinement study), $M_\infty = 0.7$, $\alpha = 149$ deg, $Re_c = 9.0 \times 10^6$.

problems associated with computations, especially in regions of large flow separation, do not plague experimental measurements, it must be acknowledged that experimental measurements do have errors that can be significant, especially in the transonic flow regime. Thus, experimental results also need validation. The best possible validation of a CFD code is by comparison with multiple independent results involving both computations and experimental data, several sets of each.

Jones Airfoil Cases

The last airfoil considered in the VTA Workshop is a supercritical-like airfoil developed by R. T. Jones at NASA Ames Research Center. This airfoil is defined by a conformal mapping procedure that has been programmed to produce a suitable tabulated definition, which is given in Ref. 17. This airfoil has neither been tested experimentally nor with CFD methods to any significant degree. It is being used in this workshop as a "blind" case. That is, there is no guidance associated with this airfoil, experimental or otherwise, that will influence the computations performed in this workshop. Experimentation with this airfoil would provide a measure of the predictive capabilities of the CFD methods described within. Hence, as of this writing, no experimentation for this airfoil is planned.

For the sake of brevity, only one Jones airfoil case is presented herein. This case is the most difficult individual calculation associated with a pressure distribution for the VTA Workshop. It involves the Jones airfoil at a particularly difficult set of conditions: $M_\infty = 0.85$, $\alpha = 2.0$ deg, and $Re_c = 9 \times 10^6$, with transition located at the airfoil leading edge. The high Mach number coupled with camber and angle of attack cause strong, shock-induced boundary-layer separation on the airfoil upper surface. A strong shock also exists on the lower surface. The computed surface pressure coefficient distributions for this case are displayed in Fig. 16 on four sets of axes. The most surprising aspect associated with this calculation is the amount of variation in the upper-surface shock position, 31% of chord, while the lower-surface variation is a respectable 9%. As can be seen from Figs. 16a–16d, the upper- and lower-surface pressure distributions upstream of each respective shock wave are in good agreement with each other. The upper-surface shock position is controlled by separation at the base of the shock. For those methods that predict a large amount of separation, which is largely controlled by the turbulence model mechanism, the shock moves forward. In addition to the large variation associated with the upper-surface shock position, the lower-surface pressure distribution downstream of the shock has a large variation. This is true for solutions that essentially agree in lower-surface shock position (see Figs. 16a, 16c, and 16d).

The lack of agreement among the various methods for the last Jones airfoil case in particular, and to a lesser extent for all cases presented with boundary-layer separation, suggests that these computations need a great deal of improvement before CFD codes can achieve design tool status in this area. Most of this lack of capability is associated with the turbulence modeling problem. An engineering turbulence model that can approximately predict the size and extent of separated regions is desperately needed.

Table 1 Summary of authors and numerical methods used in the viscous transonic airfoil workshop

No.	Author(s)	Method description
1	Sugavanam[1]	NS, modified ADI, BL
2	Desai, Rangarajan[2]	NFP + LEBL + visc ramp, SLOR + grid sequencing
3	Dargel, Thiede[3]	NFP + MIBL + nonisentropic shock-point operator
4	Rumsey, Taylor, Thomas Anderson[4]	NS, AF, upwind FV, BL
5	Melnik, Brook, Mead[5]	CFP + LEBL, MG-ADI
6	Maksymiuk, Pulliam[6]	NS, diagonal-ADI, BL
7	Coakley[7]	NS, upwind-ADI, FV, CS
8	"	NS, upwind-ADI, FV, BL
9	"	NS, upwind-ADI, FV, JK
10	"	NS, upwind-ADI, FV, $(q\text{-}\omega)$
11	Chen, Li, Alemdavoglu, Mehta, Chang, Chen, Cebeci[8,9]	Euler + BL, MG, FV, CS
12	"	NS, ADI, BL
13	"	FP + IBL, CS
14	King[10]	NS, ADI, CS
15	"	NS, ADI, BL
16	"	NS, ADI, JK
17	Huff, Wu, Sankar[11]	NS, ADI, BL
18	Matsushima, Obayashi, Fujii[12]	NS, LU-ADI, flux limiter, BL
19	Haase, Echtle[13]	NS, 3-step RK + RA, FV, CS
20	"	CFP + LEBL, MG-ADI
21	Kordulla[14]	NS, implicit pred-corr, BL
22	Drela, Giles[15]	Euler + MIBL, FV, Newton it
23	Morinishi, Satofuka[16]	NS, MG, RK, RA, BL

NS – Navier-Stokes, NFP – nonconservative full potential, CFP – conservative full potential, IBL – inverse boundary layer, LEBL – lag entrainment boundary layer, MIBL – momentum integral boundary layer, MG – multigrid, FV – finite volume, RK – Runge-Kutta, RA – residual averaging, BL – Baldwin-Lomax, JK – Johnson-King, CS – Cebeci-Smith.

Grid Refinement Study

As a part of the VTA Workshop, a grid refinement study was requested for the NACA 0012 airfoil solution presented in Fig. 1. The conditions for this solution are as follows: $M_\infty = 0.7$, $\alpha = 1.49$ deg, and $Re_c = 9 \times 10^6$. This is a relatively easy solution, with all CFD methods producing excellent agreement with each other and with experiment in terms of surface pressure (see Fig. 1). Results of the grid refinement study are shown in Fig. 17, where the drag coefficient is plotted vs the inverse of the number grid points on the airfoil chord (Δ). There are a total of six curves displayed in this figure, all without labels. The computational points defining each curve are displayed as solid circular symbols. The experimental drag level from Harris and a drag band representing the computational methods that reported drag levels for this case are also displayed. As desired, most of the curves approach a drag asymptote that falls in the lower end of the computational band near the experimental value ($C_D = 0.0079$). Of the curves presented, three have large slopes and three have small slopes. The methods that produce small-slope results have reasonable drag levels even on coarse grids, which is a desirable characteristic. The methods that produce large-slope results have large drag errors when coarse grids are used. This is an alarming situation. Grid refinement checks such as the one in Fig. 17 are extremely important and can help calibrate the level of grid refinement required for applications and even uncover errors when the proper asymptotic behavior is not achieved.

Computational Statistics

A summary of computed lift and drag coefficients from most of the numerical methods is displayed in Tables 2 and 3. Values for the NACA 0012 airfoil are displayed in Table 2, and values for the RAE 2822 airfoil are displayed in Table 3. The number on the left-hand side in each table corresponds to the method number established in Table 1 and can be used to fully identify the author(s) and method used to produce each set of force coefficients. Experimental lift and drag values are also included. Since many different angle-of-attack corrections were used for the RAE 2822 airfoil cases, actual angle-of-attack values used in each computation for each method are included in Table 3. For some methods, the freestream Mach number for the RAE 2822 airfoil cases was also "corrected." This correction was unusually small, ranging from 0 to 0.005, and, therefore, is not included. Lift and drag values for the attached cases are relatively consistent, with most values falling within the $\pm 3\%$ range for lift and $\pm 5\%$ range for drag. These ranges, which represent state-of-the-art capabilities for attached-flow lift and drag predictions, are small enough to be useful in the design environment. The weakly to moderately separated cases show more variation in lift and drag and suggest the lack of consistency for these cases.

Table 2 Summary of experimental and computational force coefficients for the NACA 0012 airfoil cases used in the viscous transonic airfoil workshop

	$M_\infty = 0.7$		$M_\infty = 0.55$		$M_\infty = 0.799$	
No.	C_L	C_D	C_L	C_D	C_L	C_D
Exp	0.241	79	0.983	253	0.390	331
2	0.249	100	1.160	360	—	—
4	0.242	74	0.990	363	0.443	413
5	0.256	83	1.109	356	—	—
6	0.254	83	0.988	362	0.472	445
7	0.253	81	0.975	350	0.429	413
8	0.255	83	0.994	358	0.476	446
9	0.235	81	0.911	333	0.300	345
10	0.253	85	0.970	344	0.434	418
11	0.245	100	1.062	—	0.412	410
12	0.243	—	0.944	—	0.461	—
13	0.252	—	1.140	—	—	—
14	0.251	82	0.989	401	0.435	414
15	0.251	80	0.973	390	0.461	429
16	0.240	84	0.920	389	0.324	350
19	—	—	0.968	365	0.397	386
20	0.262	82	—	—	—	—
22	0.251	82	0.913	298	0.312	337

All drag coefficient values are in terms of drag counts: $C_D = 1$ count is equivalent to $C_D = 0.0001$.

Table 3 Summary of experimental and computational force coefficients for the RAE 2822 airfoil cases used in the viscous transonic airfoil workshop (cases 6 and 10 from Ref. 26)

	$M_\infty = 0.725$			$M_\infty = 0.75$		
No.	C_L	C_D	α, deg	C_L	C_D	α, deg
Exp	0.743	127	2.92	0.743	242	3.19
2	0.749	122	2.80	—	—	2.70
3	0.740	131	2.56	0.740	230	2.96
4	0.752	136	2.54	0.809	278	2.81
5	0.755	126	2.54	0.773	293	2.81
6	0.747	123	2.30	0.838	289	2.72
7	0.768	119	2.40	0.815	269	2.80
8	0.788	124	2.40	0.859	298	2.80
9	0.717	113	2.40	0.745	243	2.80
10	0.773	125	2.40	0.836	284	2.80
11	0.756	180	2.60	0.746	250	2.70
12	0.738	—	2.59	0.751	—	2.55
13	0.744	—	2.52	0.743	—	2.50
14	—	—	—	0.795	271	2.80
15	—	—	—	0.813	279	2.80
16	—	—	—	0.742	250	2.80
19	0.749	144	2.47	0.793	281	2.74
20	0.822	132	2.47	—	—	—
22	0.723	113	2.44	0.733	224	2.70

All drag coefficient values are in terms of drag counts: $C_D = 1$ count is equivalent to $C_D = 0.0001$.

A relatively complete set of computational statistics for several of the cases just presented is given in Ref. 17. Of particular interest are the floating-point operation counts required for a solution from each of the individual methods. These statistics were not directly available from each author but were estimated from the statistics generally supplied by each author. The variation in per-solution operation count was quite large, ranging from 4×10^7 to 6×10^{11}. The inviscid-plus-boundary-layer methods (nos. 2, 3, 5, 11, 13, 20, and 22 from Table 1) have operation counts that range from about 4×10^7 to 2×10^{10}. This range is very large by itself and is primarily due to the wide diversity of methods within this category. The operation counts for the Navier-Stokes methods vary from about 2×10^{10} to 6×10^{11} and are due to variations in grid size and rates of convergence. From these statistics, the inviscid-plus-boundary-layer methods appear to be about 30–500 times faster than the Navier-Stokes methods. However, caution should be exercised with this comparison because the Navier-Stokes methods generally utilized finer grids and produced most of the solutions for the more difficult cases, e.g., cases involving maximum lift or drag. In addition, several of the Navier-Stokes methods were used time-accurately for unsteady solutions, which increased the operation counts for these runs by several times.

Concluding Remarks

The VTA Workshop has been held for the purpose of validating viscous transonic airfoil computations over a range of geometries and flow conditons. A total of 15 author groups have submitted 23 different sets of computed results. These results are compared with each other and experiment, when appropriate, in a series of plots and tables. The primary objective of this presentation is to establish method capabilities for predicting trends and individual flowfield details. An additional purpose is the establishment of a data base that can be used for future computer code validation.

To a large extent the results obtained from the VTA Workshop are presented herein without concluding remarks. Specific conclusions about which methods are superior or inferior are left to the reader. Nevertheless, several general conclusions are easily identified and are now presented.

1) CFD methods for transonic, attached airfoil calculations have reached a sophisticated level of development. Most methods are capable of producing valuable results in the design environment, including the prediction to lift of within $\pm 3\%$ and drag to within $\pm 5\%$. Other computed flow-field data, including velocity boundary-layer profiles and skin-friction distributions, are in good agreement with each other and with experiment. Computational and experimental scatter for zero-lift drag-rise chacteristics are comparable.

2) CFD methods for transonic, separated airfoil calculations are not as well developed as the methods for attached flow computations. This is largely due to the lack of accurate turbulence modeling in regions of separated flow. Turbulence model inadequacies are the most important physical model error associated with the results contained in this report. Despite this major problem, recent progress in this area suggests hope for the future.

3) Many errors associated with CFD computer programs are solely numerical in nature. This type of error can be identified by various types of solution-to-solution comparison. Inappropriate grid clustering and refinement are the most important numerical errors associated with the results contained in this report. Establishment of "standard" levels of grid refinement is difficult because different methods have different requirements. However, grid refinement studies can be used to help eliminate these errors. More emphasis should be placed on solution-to-solution comparisons to aid in the evaluation and elimination of numerical errors.

Acknowledgments

The time and effort of all the authors who participated in this workshop is deeply appreciated. Without their efforts, an undertaking of this sort would not have been possible. In addition, the selection of test cases used in this workshop was done by committee members: Drs. Richard Barnwell, Leland Carlson, Norman Malmuth, Frank Marconi, Jr., William McCroskey, and William Van Dalsem. Their efforts are deeply appreciated.

References

[1]Sugavanam, A., "Transonic Viscous Flow Predictions with the Lockheed Navier-Stokes Code," AIAA Paper 87-0410, Jan. 1987.

[2]Desai, S. S. and Rangarajan, R., "Viscous Transonic Flow over Aerofoils Using Transonic Full Potential Equation in a System of Cartesian Coordinates," AIAA Paper 87-0411, Jan. 1987.

[3]Dargel, G. and Thiede, P., "Viscous Transonic Airfoil Simulation by an Efficient Viscous-Inviscid Interaction Method," AIAA Paper 87-0412, Jan. 1987.

[4]Rumsey, C. L., Taylor, S. L., Thomas, J. L., and Anderson, W. K., "Application of an Upwind Navier-Stokes Code to Two-Dimensional Transonic Airfoil Flow," AIAA Paper 87-0413, Jan. 1987.

[5]Melnik, R., Brook, J., and Mead, H., "GRUMFOIL: A Computer Code for the Computation of Viscous Transonic Flow Over Airfoils," AIAA Paper 87-0414, Jan. 1987.

[6]Maksymiuk, C. M. and Pulliam, T. H., "Viscous Transonic Airfoil Workshop Results Using ARC2D," AIAA Paper 87-0415, Jan. 1987.

[7]Coakley, T. J., "Numerical Simulation of Viscous Transonic Airfoil Flows," AIAA Paper 87-0416, Jan. 1987.

[8]Chen, L. T., Li, S., and Chen, H., "Calculation of Transonic Airfoil Flows by Interaction of Euler and Boundary-Layer Equations," AIAA Paper 87-0521, Jan. 1987.

[9]Chang, K. C., Alemdaroglu, N., Mehta, U., and Cebeci, T., "Further Comparisons of Interactive Boundary-Layer and Thin-Layer Navier-Stokes Procedures," AIAA Paper 87-0430, Jan. 1987.

[10]King, L. S., "A Comparison of Turbulence Closure Models for Transonic Flows About Airfoils," AIAA Paper 87-0418, Jan. 1987.

[11]Huff, D. L., Wu, J.- C., and Sankar, L. N., "Analysis of Viscous Transonic Flow Over Airfoil Sections, AIAA Paper 87-0420, Jan. 1987.

[12]Matsushima, K., Obayashi, S., and Fujii, K., "Navier-Stokes Computations of Transonic Flow Using the LU-ADI Method," AIAA Paper 87-0421, Jan. 1987.

[13]Haase, W., Stock, H.- W., and Echtle, H., "Computational Results for Some Test Cases of Viscous Transonic Flow Around Airfoils," AIAA Paper 87-0422, Jan. 1987.

[14]Kordulla, W., "Using an Unfactored Predictor-Corrector Method," AIAA Paper 87-0423, Jan. 1987.

[15]Drela, M. and Giles, M., "Viscous-Inviscid Analysis of Transonic and Low Reynolds Number Airfoils," AIAA Paper 87-0424, Jan. 1987.

[16]Morinishi, K. and Satofuka, N., "A Numerical Study of Viscous Transonic Flows Using RRK Scheme," AIAA Paper 87-0426, Jan. 1987.

[17]Holst, T. L., "Viscous Transonic Airfoil Workshop Compendium of Results," AIAA Paper 7-1640, Jan. 1987.

[18]Kline, S. J., Cantwell, B. J., and Lilley, G. M., *Complex Turbulent Flows*, Vol. 2, 1980–81, AFOSR-HTTM-Stanford Conference on Complex Turbulent Flows, Stanford Univ., CA, 1982.

[19]Harris, C. D., "Two-Dimensional Aerodynamic Characteristics of the NACA 0012 Airfoil in the Langley 8-Foot Transonic Pressure Tunnel," NASA TM-81927, 1981.

[20]Baldwin, B. S. and Lomax, H., "Thin Layer Approximation and Algebraic Model for Separated Turbulent Flows," AIAA Paper 78-0257, Jan. 1978.

[21]Cebeci, T. and Smith, A. M. O., *Analysis of Turbulent Boundary Layers*, Academic, New York, 1974.

[22]Johnson, D. A. and King, L. S., "A Mathematically Simple Turbulence Closure Model for Attached and Separated Turbulent Boundary Layers," *AIAA Journal*, Vol. 23, Nov. 1985, pp. 1684–1692.

[23]Coakley, T. J., "Turbulence Modeling Methods for the Compressible Navier-Stokes Equations," AIAA Paper 83-1693, July 1983.

[24]McCroskey, W. J., private communication, Oct. 1987.

[25]McCroskey, W. J., "A Critical Assessment of Wind Tunnel Results for the NACA 0012 Airfoil," Paper 1, AGARD Fluid Dynamics Panel Symposium on Aerodynamic Data Accuracy and Quality: Requirements and Capabilities in Wind Tunnel Testing, Naples, Italy, Sept.-Oct. 1987.

[26]Cook, P. H., McDonald, M. A., and Firmin, M. C. P., "Aerofoil RAE 2822—Pressure Distributions, and Boundary Layer and Wake Measurements," AGARD-AR-138, 1979.